INTERNATIONAL JOURNAL FOR NUMERICAL METHODS IN FLUIDS, VOL. 23, 241–269 (1996)

FULLY DISCRETE HIGH-ORDER SHOCK-CAPTURING NUMERICAL SCHEMES

J. SHI

Department of Civil Engineering, Queen Mary and Westfield College, Mile End Road, London, U.K.

AND

E. F. TORO

Department of Mathematics and Physics, Manchester Metropolitan University, Chests Street, Manchester, U.K.

SUMMARY

The present paper is a sequel to a previous one by the same authors in which a family of up to fourth-order fully discrete (FD) upwind numerical schemes was presented. In this paper we extend those high-order FD schemes to solutions with discontinuities, e.g. shocks. A rigorous anlaysis of the total variation diminishing (TVD) constraint for the high-order FD schemes is carried out. For non-linear systems the TVD constraint is, as usual, applied empirically. These schemes are validated by solving a test problem for the time-dependent shallow water equations.

KEY WORDS: fully discrete; high-order; conservative; upwind; shock-capturing; TVD

1. INTRODUCTION

In Reference 1 we established a fully discrete methodology from which two-level explicit arbitrary-order conservative upwind schemes can be derived. However, these schemes are only suitable for linear systems or non-linear systems with smooth solutions. It is well known that in solving non-linear systems with shocks, such as transonic flows, when applying high-order schemes it is inevitable that oscillations will be observed in the vicinity of the shocks, which might trigger instabilities. The mechanism behind the oscillations was well discussed by Trefethen.[2] It turns out that the oscillations are caused by the dispersion of the highly oscillatory wave components which are associated with high wave numbers of the Fourier spectrum. This problem had frustrated people for many years until the concept and theory of total variation diminishing (TVD) schemes was introduced.[3] Since then a variety of second-order TVD schemes have been developed.[4]

In this paper the TVD theory is applied to the conservative upwind higher-order fully discrete (FD) schemes presented in Reference 1. These high-order TVD schemes can avoid spurious oscillations and preserve high-order accuracy in smooth parts of the flow. This is achieved by imposing a TVD constraint via the introduction of flux limiter functions.[4] For second-, third- and fourth-order-accurate schemes a rigorous TVD analysis that results in Courant-number-dependent TVD regions is carried out. Flux limiter functions are constructed and tested. For methods of higher oder of accuracy a

CCC 0271–2091/96/030241–29

Received May 1995
Revised November 1995

semiempirical TVD approach that works well is proposed. The extension of these high-order TVD schemes to non-linear hyperbolic conservation laws is validated by solving a test problem for the time-dependent one-dimensional shallow water equations.

The rest of this paper is organized as follows. In Section 2 the TVD concept is discussed. In Section 3 the TVD theory for fully discrete schemes is investigated. In Section 4 the TVD theory is applied to derive Courant-number-dependent TVD regions and to construct and test limiter functions for second-order methods. In Sections 5 and 6 the TVD theory is applied to third- and fourth-order fully discrete schemes. In Section 7 a semiempirical procedure to develop TVD versions of schemes of arbitrary order of accuracy is investigated. In Section 8 the extension of the high-order schemes to non-linear hyperbolic systems is presented. Conclusions are drawn in Section 9.

2. TOTAL VARIATION STABILITY

The total variation $TV(U^{n+1})$ of the discrete solution is defined as

$$TV(U^{n+1}) = \sum_j |U_{j+1}^{n+1} - U_j^{n+1}|. \tag{1}$$

Under this definition a numerical method is called total variation diminishing if the following condition is satisfied:

$$TV(U^{n+1}) \leqslant TV(U^n), \tag{2}$$

which simply states that the total variation is not increased as time evolves, so that $TV(U^n)$ at any time n is bounded by $TV(U^0)$ of the initial data.

For a consistent, conservative and entropy-satisfying method for a scalar conservation law, provided that the condition of inequality (2) is satisfied, the solution will converge to the correct weak solution.

To apply the TVD concept, we use Harten's theorem,[3] which states that a scheme written as

$$U_j^{n+1} = U_j^n - B_{j-1/2}\Delta U_{j-1/2} + D_{j+1/2}\Delta U_{j+1/2} \tag{3}$$

is TVD provided that

$$B_{j-1/2} \geqslant 0, \tag{4}$$

$$D_{j+1/2} \geqslant 0, \tag{5}$$

$$B_{j-1/2} + D_{j+1/2} \leqslant 1. \tag{6}$$

Another more convenient and practical criterion for applying the TVD concept is provided by Roe's data compatibility condition:[5]

$$0 \leqslant \frac{U_j^{n+1} - U_j^n}{U_{j-1}^n - U_j^n} \leqslant 1 \quad \text{for } 0 \leqslant c \leqslant 1, \tag{7}$$

$$0 \leqslant \frac{U_j^{n+1} - U_j^n}{U_{j+1}^n - U_j^n} \leqslant 1 \quad \text{for } -1 \leqslant c \leqslant 0. \tag{8}$$

3. TVD ANALYSIS FOR HIGH-ORDER FD SCHEMES

The initial value problem (IVP) for the one-dimensional scalar hyperbolic conservation laws is considered, namely

$$\begin{aligned} &u_t + f(u)x = 0, \quad -\infty < x < \infty, \quad t \geqslant 0, \\ &u(x, 0) = u_0(x). \end{aligned} \tag{9}$$

Here u is the unknown function and $f(u)$ is the physical flux.

First let us consider the linear case $f(u) = au$ so that $f'(u) = a$ is a constant wave propagation speed.

The conservation numerical schemes introduced in Reference 1 have the form

$$U_j^{n+1} = U_j^n - \frac{k}{h}(F_{j+1/2} - F_{j-1/2}), \tag{10}$$

with numerical flux

$$F_{j+1/2} = \tfrac{1}{2}(F_j^n + F_{j+1}^n) - \tfrac{1}{2}|a|\Delta U_{j+1/2} + |a|(D_0\Delta U_{j+1/2} + D_1\Delta U_{j+L+1/2} + D_2\Delta U_{j+M+1/2}), \tag{11}$$

where D_0, D_1 and D_2 are coefficients, k is the time step, h is the mesh width, the notation $F_{j+1/2}$ is equivalent to $F(U^n; j)$ in Reference 1 and

$$\Delta U_{j+q+1/2} = U_{n+q+1}^n - U_{j+q}^n \quad (q = 0, L, M), \tag{12}$$

$$L = -1 \quad \text{and} \quad M = 1 \quad \text{for } c > 0, \qquad L = 1 \quad \text{and} \quad M = -1 \quad \text{for } c < 0. \tag{13}$$

Here $c = ak/h$ is the Courant number. The above flux incluedes three-point second-order space-centred schemes, five-point second-order upwind schemes, five-point third-order upwind-biased schemes and five-point fourth-order space-centred schemes. For example, when

$$D_1 = D_2 = 0, \qquad D_0 = (1 - |c|)/2, \tag{14}$$

a second-order space-centred schemes is obtained which has the stability condition $|c| \leqslant 1$; when

$$D_0 = D_2 = 0, \qquad D_1 = (1 - |c|)/2, \tag{15}$$

a second-order upwind scheme is obtained which has the stability condition $|c| \leqslant 2$; when

$$D_2 = 0, \qquad D_1 = (1 - c^2)/6, \qquad D_0 = \tfrac{1}{3} - |c|/2 + c^2/6, \tag{16}$$

a five-point third-order upwind-biased scheme is obtained which has the stability condition $|c| \leqslant 1$; when

$$\begin{aligned} &D_0 = \tfrac{1}{2} - 7|c|/12 + |c^3|/12, \qquad D_1 = \tfrac{1}{12} + |c|/24 - c^2/12 - |c^3|/24, \\ &D_2 = c^2/12 + |c|/24 - \tfrac{1}{12} - |c^3|/24, \end{aligned} \tag{17}$$

a five-point fourth-order space-centred scheme is obtained which has the stability condition $|c| \leqslant 1$.

Imposing a TVD constraint on (11) via flux limiter functions gives

$$F_{j+1/2} = \tfrac{1}{2}(F_j^n + F_{j+1}^n) - \tfrac{1}{2}|a|U_{j+1}^n - U_j^n) + |a|(D_0\Delta U_{j+1/2} + D_1\Delta U_{j+L+1/2})\phi_j + |a|D_2\Delta U_{j+M+1/2}\phi_{j+M}, \tag{18}$$

where ϕ_j and ϕ_{j+M} are flux limiter functions.

Theorem

Scheme (10), (18), is TVD for $|c| \leqslant 1$ if the limiter function is determined by

$$\phi_j \leqslant \frac{(1-|c|)\theta_j}{\eta(D_1\theta_j + D_0 - D_2)}, \tag{19}$$

$$\phi_j \leqslant \frac{1-|c|+\eta D_2/\theta_j^*}{\eta(D_0 + D_1\theta_j)}, \tag{20}$$

$$\phi_j \geqslant \frac{D_2}{(D_0 + D_1\theta_j)\theta_j^*}, \tag{21}$$

$$\phi_j \geqslant 0, \tag{22}$$

where θ_j is called the local flow parameter and is defined by

$$\theta_j = \Delta U_{j-1/2}/\Delta U_{j+1/2} \quad \text{for } c > 0, \tag{23}$$

$$\theta_j = \Delta U_{j+3/2}/\Delta U_{j+1/2} \quad \text{for } c < 0, \tag{24}$$

θ_j^* is called the upwind–downwind flow parameter and is given by

$$\theta_j^* = \Delta U_{j-1/2}/\Delta U_{j+3/2} \quad \text{for } c > 0, \tag{25}$$

$$\theta_j^* = \Delta U_{j+3/2}/\Delta U_{j-1/2} \quad \text{for } c < 0, \tag{26}$$

and η is defined by

$$\eta = \begin{cases} 1-|c| & \text{for } 0 \leqslant |c| < \frac{1}{2}, \\ |c| & \text{for } \frac{1}{2} \leqslant |c| \leqslant 1. \end{cases} \tag{27}$$

Proof. First consider a method with Courant number $0 \leqslant c \leqslant 1$. From (10) and (18) the numerical method is

$$\begin{aligned} U_j^{n+1} = U_j^n - c(&\Delta U_{j-1/2} + D_0\Delta U_{j+1/2}\phi_j + D_1\Delta U_{j-1/2}\phi_j - D_0\Delta U_{j-1/2}\phi_{j-1} \\ &- D_1\Delta U_{j-3/2}\phi_{j-1} - D_2\Delta U_{j+1/2}\phi_j + D_2\Delta U_{j+3/2}\phi_{j+1}). \end{aligned} \tag{28}$$

Modifying equation (28), we have

$$\frac{U_j^{n+1} - U_j^n}{-\Delta U_{j-1/2}} = c\left[1 + \left(D_1 + (D_0 - D_2)\frac{1}{\theta_j}\right)\phi_j - (D_0 + D_1\theta_{j-1})\phi_{j-1} + D_2\frac{1}{\theta_j^*}\phi_{j+1}\right]. \tag{29}$$

We now apply the data compatibility condition of equation (7) whereby the sufficient condition

$$0 \leqslant \frac{U_j^{n+1} - U_j^n}{-\Delta U_{j-1/2}} \leqslant 1 \tag{30}$$

satisfies the TVD requirement.

This is equivalent to Harten's theorem (3)–(6) with the choice

$$B_{j-1/2} = c\left[1 + \left(D_1 + (D_0 - D_2)\frac{1}{\theta_j}\right)\phi_j - (D_0 + D_1\theta_{j-1})\phi_{j-1} + D_1\frac{1}{\theta_j^*}\phi_{j+1}\right], \qquad D_{j+1/2} = 0.$$

We apply condition (30) to (29), i.e.

$$0 \leqslant c\left[1 + \left(D_1 + (D_0 - D_2)\frac{1}{\theta_j}\right)\phi_j - (D_0 + D_1\theta_{j-1})\phi_{j-1} + D_2\frac{1}{\theta_j^*}\phi_{j+1}\right] \leqslant 1. \tag{31}$$

One way to satisfy these inequalities is by imposing

$$\left(D_1 + (D_0 - D_2)\frac{1}{\theta_j}\right)\phi_j - \left((D_0 + D_1\theta_{j-1})\phi_{j-1} - D_2\frac{1}{\theta_j^*}\phi_{j+1}\right) \leqslant \frac{1-c}{c}, \tag{32}$$

$$\left((D_0 + D_1\theta_{j-1})\phi_{j-1} - D_2\frac{1}{\theta_j^*}\phi_{j+1}\right) - \left(D_1 + (D_0 - D_2)\frac{1}{\theta_j}\right)\phi_j \leqslant 1, \tag{33}$$

i.e.

$$0 \leqslant \left(D_1 + (D_0 - D_2)\frac{1}{\theta_j}\right)\phi_j \leqslant \frac{1-c}{c}, \tag{34}$$

$$0 \leqslant (D_0 + D_1\theta_{j-1})\phi_{j-1} - D_2\frac{1}{\theta_j^*}\phi_{j+1} \leqslant \frac{1-c}{c}, \tag{35}$$

$$0 \leqslant \left(D_1 + (D_0 - D_2)\frac{1}{\theta_j}\right)\phi_j \leqslant 1, \tag{36}$$

$$0 \leqslant (D_0 + D_1\theta_{j-1})\phi_{j-1} - D_2\frac{1}{\theta_j^*}\phi_{j+1} \leqslant 1. \tag{37}$$

This leads to the following conditions on the flux limiter:

$$\phi_j \leqslant \frac{(1-c)\theta_j}{c(D_1\theta_j + D_0 - D_2)}, \tag{38}$$

$$\phi_j \leqslant \frac{\theta_j}{D_1\theta_j + D_0 - D_2}, \tag{39}$$

$$\phi_j \leqslant \frac{1 - c + cD_2\phi_{j+1}/\theta_j^*}{c(D_0 + D_1\theta_j)}, \tag{40}$$

$$\phi_j \leqslant \frac{1 + D_2\phi_{j+1}/\theta_j^*}{D_0 + D_1\theta_j}, \tag{41}$$

$$\phi_j \geqslant \frac{D_2\phi_{j+1}}{(D_0 + D_1\theta_j)\theta_j^*}. \tag{42}$$

$$\phi_j \geqslant 0 \tag{43}$$

The most restrictive conditions of inequalities (38)–(41) give

$$\phi_j \leqslant \frac{(1-c)\theta_j}{\eta(D_1\theta_j + D_0 - D_2)}, \tag{44}$$

$$\phi_j \leqslant \frac{1 - c + \eta D_2\phi_{j+1}/\theta_j^*}{\eta(D_0 + D_1\theta_j)}, \tag{45}$$

where η is defined by equation (27). The analysis for $-1 \leqslant c \leqslant 0$ goes through in exactly the same way, but c is replaced by $|c|$ and ϕ_{j+1} is replaced by ϕ_{j-1}. Finally, by setting $\phi_{j+1} = 1$ or $\phi_{j-1} = 1$, the theorem is established.

In the following sections we will use the theorem to construct second-, third- and fourth-order TVD schemes.

4. SECOND-ORDER TVD SCHEME

The fully discrete second-order numerical flux (see (14)) with limiter function can be written as

$$F_{j+1/2} = \frac{1}{2}(F_j^n + F_{j+1}^n) - \frac{|a|}{2}\Delta U_{j+1/2} + \frac{|a|}{2}(1 - |c|)\Delta U_{j+1/2}\phi_j. \tag{46}$$

From equations (19)–(22) the flux limiter function ϕ_j has to satisfy the constraints

$$\phi_j \leqslant 2\theta_j/\eta, \tag{47}$$

$$\phi_j \leqslant 2/\eta, \tag{48}$$

$$\phi_j \geqslant 0. \tag{49}$$

When $\theta_j < 0$, $\phi_j < 0$ and the scheme reduces locally to first order by assuming $\phi_j = 0$.

Equations (47) and (48) indicate that the second-order TVD region is a function of the Courant number $|c|$. This conclusion is consistent with that of other researchers.[6,7] The Courant-number-dependent TVD regions of (47) and (48) are shown in Figure 1. The upper boundary of the TVD region is maximum for the choice $|c| = \frac{1}{2}$. Sweby's TVD region[4] is the special case of $|c| = 1$ in the Courant-number-dependent TVD region of Figure 1. A variety of limiters have been developed within the region.[4] However, we expect that better limiters could be constructed if we fully use the Courant-number-dependent TVD region (see Figure 1).

One limiter function called FD2A (fully discrete second-order A) has the form

$$\phi_j(\theta_j) = \max\left[0, \min\left(1, \frac{\theta_j}{\eta}\right), \min\left(\theta_j, \frac{1}{\eta}\right)\right]. \tag{50}$$

The shaded part in Figure 2 illustrates the limiter function (50). When $\eta = \frac{1}{2}$, the limiter follows the upper boundary of the area, which is Roe's SUPERBEE limiter; when $\eta = 1$, the limiter function follows the lower boundary, which is the MINMOD limiter; for other values of η the limiter function varies between SUPERBEE and MINMOD.

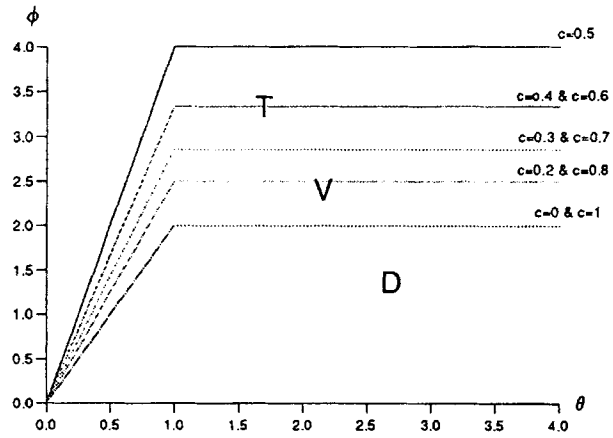

Figure 1. Courant-number-dependent second-order TVD region

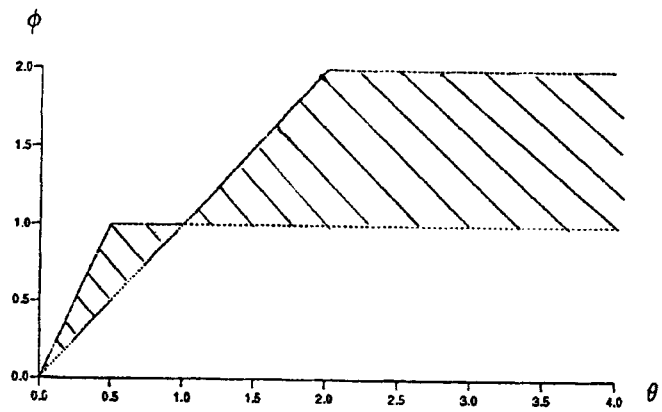

Figure 2. FD2A limiter (shaded part)

Figures 3 and 4 show a comparison of the numerical results using FD2A (symbol) and the exact solution (line). The initial condition consists of half a sine wave and a squared wave. The cell width $\Delta x = 0{\cdot}1$ is fixed. The Courant numbers used are 0·5, 0·7 and 0·9. The results are shown after 50 time steps (Figure 3) and 1000 time steps (Figure 4). Another limiter function is FD2B given by

$$\phi_j(\theta_j) = \max\left[0, \min\left(1, \frac{2\theta_j}{\eta}\right), \min\left(\theta_j, \frac{2}{\eta}\right)\right]. \tag{51}$$

This is illustrated by the shaded area of Figure 5. Note that the lower boundary now is the SUPERBEE limiter.

Figure 6 shows a comparison between the numerical results of FD2B (symbol) and the exact solution (line) after 50 time steps. For discontinuities, FD2B is superior to FD2A. Clipping of extrema in the smooth solution is less sever than that of FD2A. The tendency to 'square' smooth parts is present in both limiters and this is typical of very compressive limiters.

To illustrate the long-time behaviour of the resulting scheme, Figure 7 shows a comparison of the numerical results using SUPERBEE (cross), FD2B (square) and the exact solution (line) after 1000 time steps. As seen in the figure, the performance of FD2B for the discontinuous part of the solution is superior to that of SUPERBEE; for the smooth part of the solution they both tend to square the profile, but FD2B shows less 'clipping' of extrema. The difference between SUPERBEE and FD2B is more noticeable as the Courant number tends to $\frac{1}{2}$.

5. THIRD-ORDER TVD SCHEME

The five-point third-order scheme has the form (see (16)) for the unlimited case)

$$F_{j+1/2} = \tfrac{1}{2}(F_j^n + F_{j+1}^n) - \frac{|a|}{2}\Delta U_{j+1/2} + \left[|a|\left(\frac{1}{3} - \frac{|c|}{2} + \frac{c^2}{6}\right)\Delta U_{j+1/2} + \frac{|a|}{6}(1-c^2)\Delta U_{j+L+1/2}\right]\phi_j. \tag{52}$$

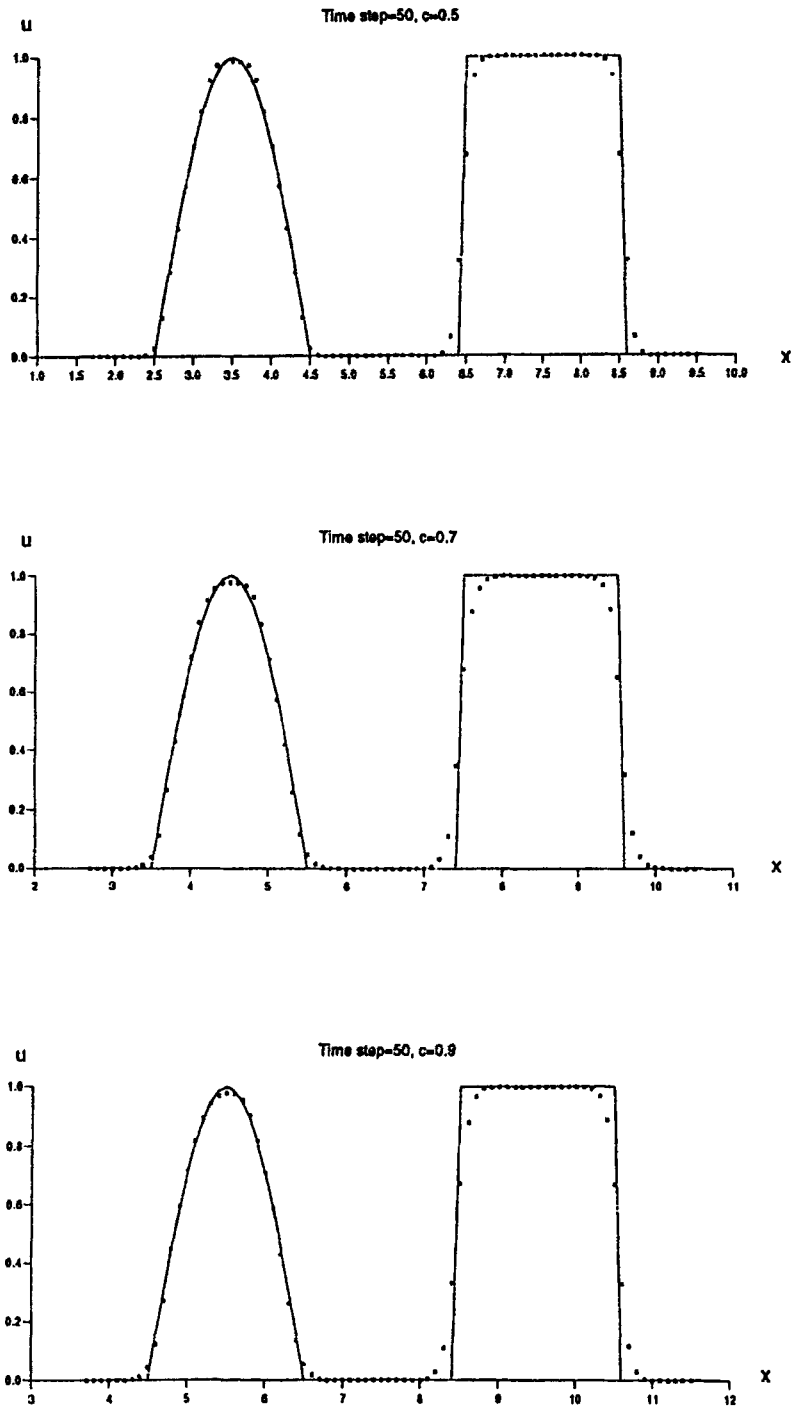

Figure 3. Comparison between exact solution (line) and numerical results of FD2A (symbol) after 50 time steps

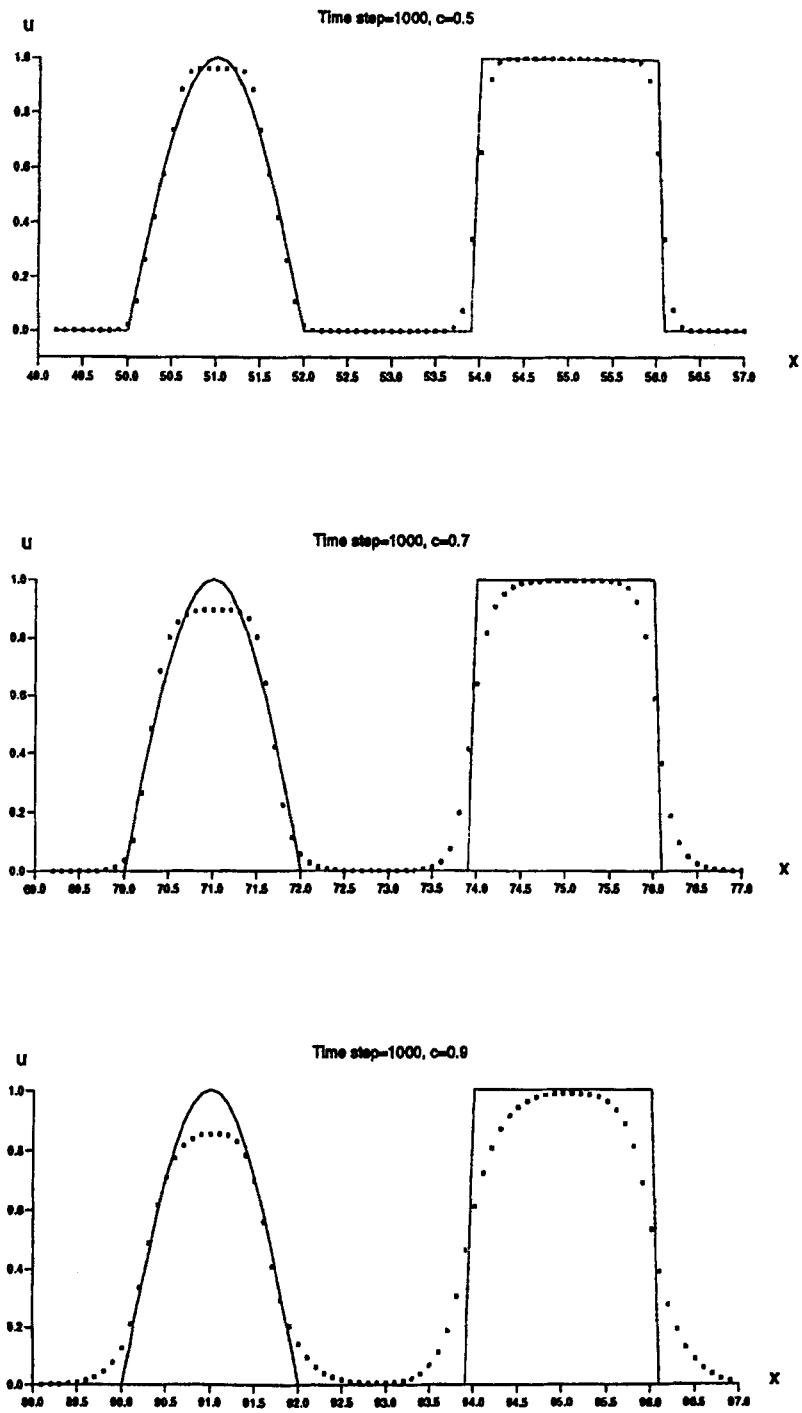

Figure 4. Comparison between exact solution (line) and numerical results of FD2A (symbol) after 1000 time steps

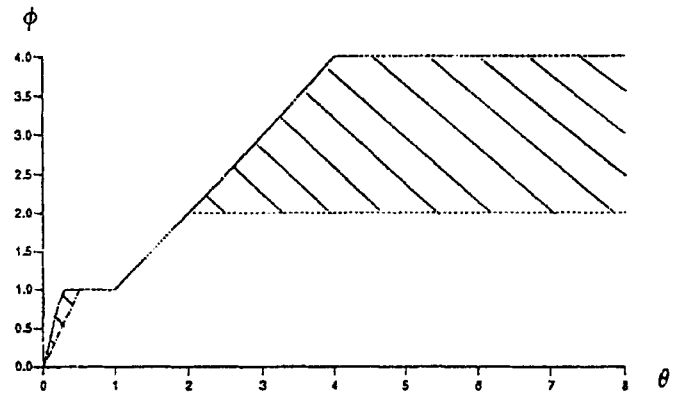

Figure 5. FD2B limiter (shaded part)

From equations (19)–(22) the limiter functions are determined by

$$\phi_j \leqslant \frac{6\theta_j}{\eta[\theta_j(1+|c|)+2-|c|]}, \tag{53}$$

$$\phi_j \leqslant \frac{6}{\eta[\theta_j(1+|c|)+2-|c|]}, \tag{54}$$

$$\phi_j \leqslant 0. \tag{55}$$

Figure 8 shows the Courant-number-dependent TVD regions of this scheme, which have similar features to those of the second-order scheme. The upper boundary of the TVD region is maximum when $|c| = \frac{1}{2}$ and minimum when $|c| = 1$. The lower boundary is always $\phi = 0$.

We can define different third-order flux limiter functions using the Courant-number-dependent TVD regions. A general limiter function for the third-order scheme called FD3 (fully discrete third-order) has the form

$$\phi_j = \begin{cases} \dfrac{6\theta_j}{\eta[\theta_j(1+|c|)+2-|c|]} & \text{if } 0 \leqslant \theta_j > \theta^{\mathrm{L}}, \\ 1 & \text{if } \theta^{\mathrm{L}} \leqslant \theta_j \leqslant \theta^{\mathrm{R}}, \\ \dfrac{6}{\eta[\theta_j(1+|c|)+2-|c|]} & \text{if } \theta_j > \theta^{\mathrm{R}}, \\ 0 & \text{if } \theta_j < 0. \end{cases} \tag{56}$$

In particular we choose a limiter function called FD3A by taking

$$\theta_{\mathrm{L}} = \frac{\eta(2-|c|)}{6-\eta(1+|c|)}, \tag{57}$$

$$\theta_{\mathrm{R}} = \frac{6-\eta(2-|c|)}{\eta(1+|c|)}. \tag{58}$$

Figure 9 shows the FD3A limiter function for three values of Courant number. They are given by the full lines.

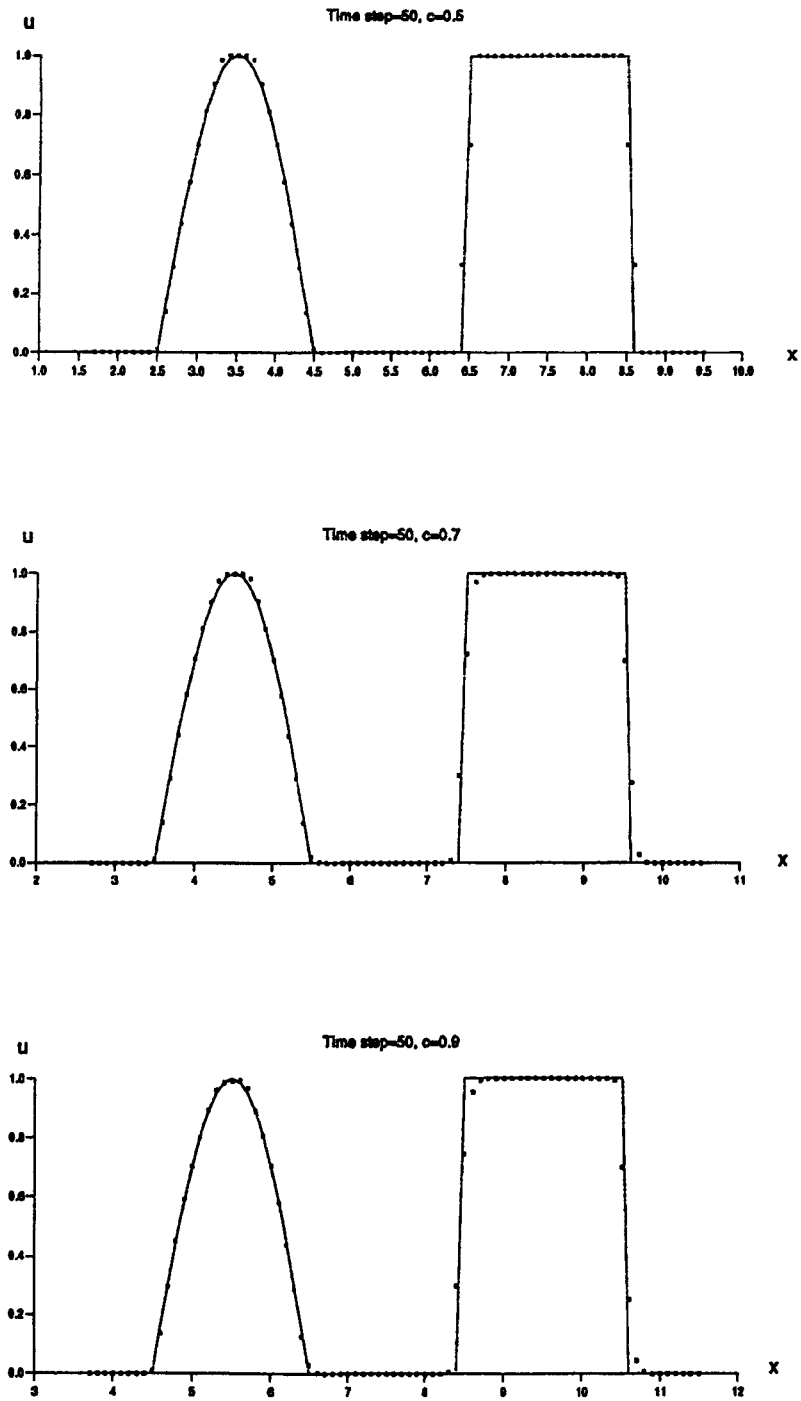

Figure 6. Comparison between exact solution (line) and numerical results of FD2B (symbol) after 50 time steps

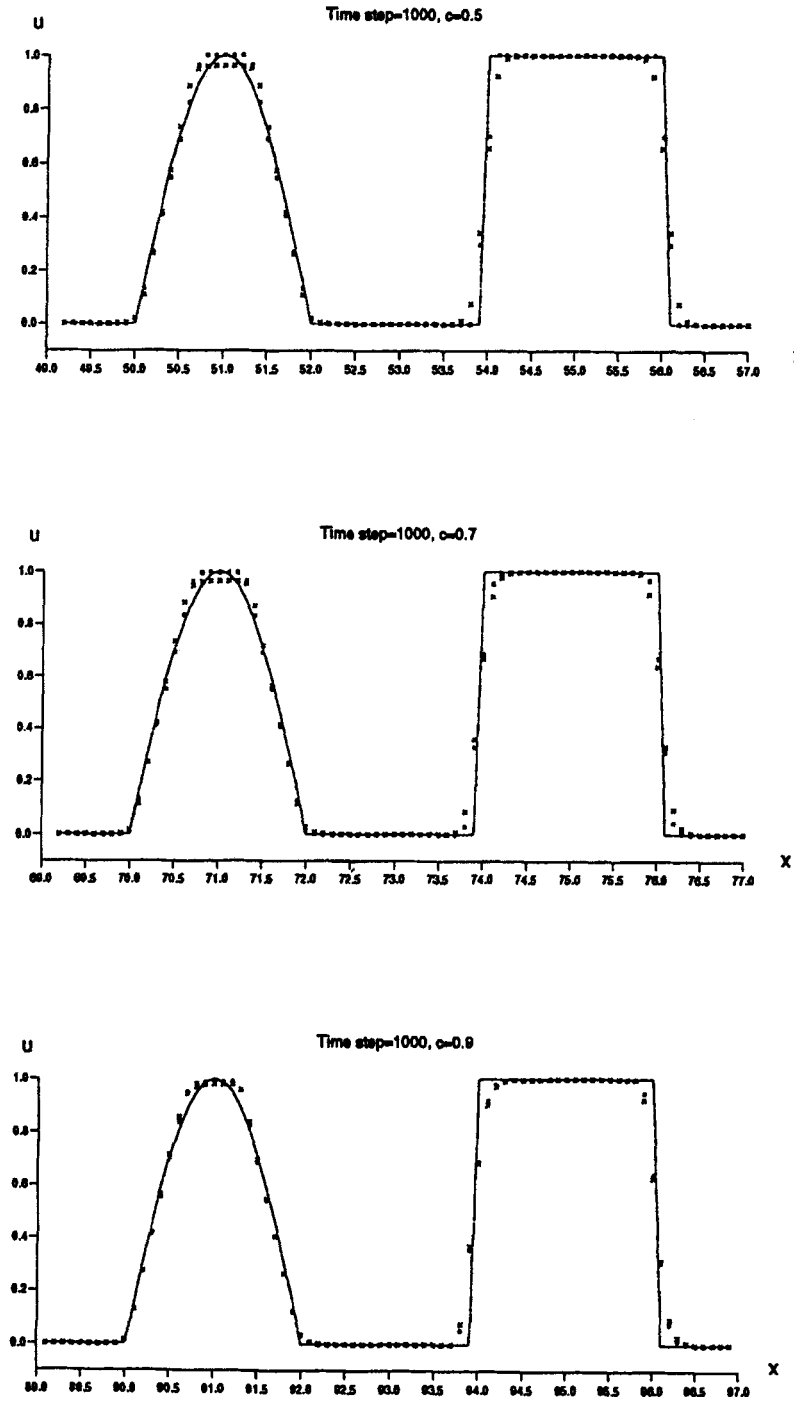

Figure 7. Comparison between exact solution (line) and numerical results of SUPERBEE (cross) and FD2B (square) after 1000 time steps

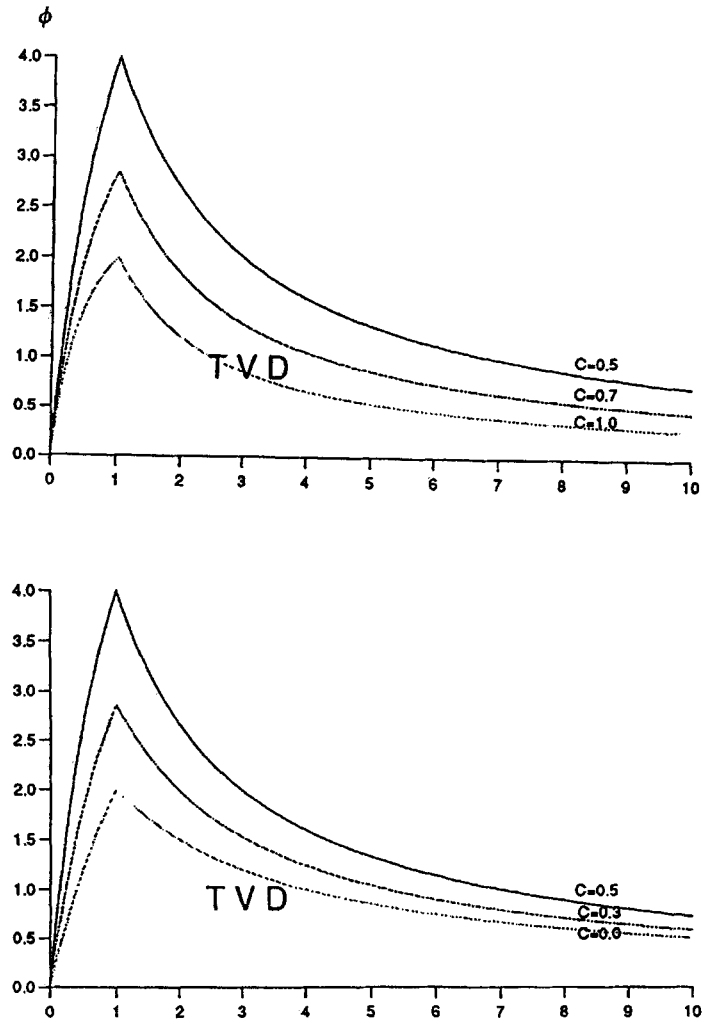

Figure 8. Courant-number-dependent third-order TVD region

Figure 10 shows the performance of the FD3A limiter function for the same test problem as before after 50 time steps with Courant numbers 0·5, 0·7 and 0·9. The solid line is the exact solution. The numerical results (symbol) are accurate in the smooth part, but discontinuities are smeared with four or five interior points. We are interested in the behaviour of the scheme for long-time evolution. Figure 11 gives the results after 1000 time steps, showing that this limiter is not very satisfactory for long times; it introduces too much numerical diffusion. Recall that owing to the imposition of the TVD property the scheme reduces locally to first-order accuracy near extrema. We suggest the limiter function FD3B given by

$$\theta^{\mathrm{L}} = 1{\cdot}1\eta - 0{\cdot}17, \tag{59}$$

$$\theta^{\mathrm{R}} = 2{\cdot}78 - 1{\cdot}4\eta. \tag{60}$$

Figure 12 shows FD3B for Courant number 0·5.

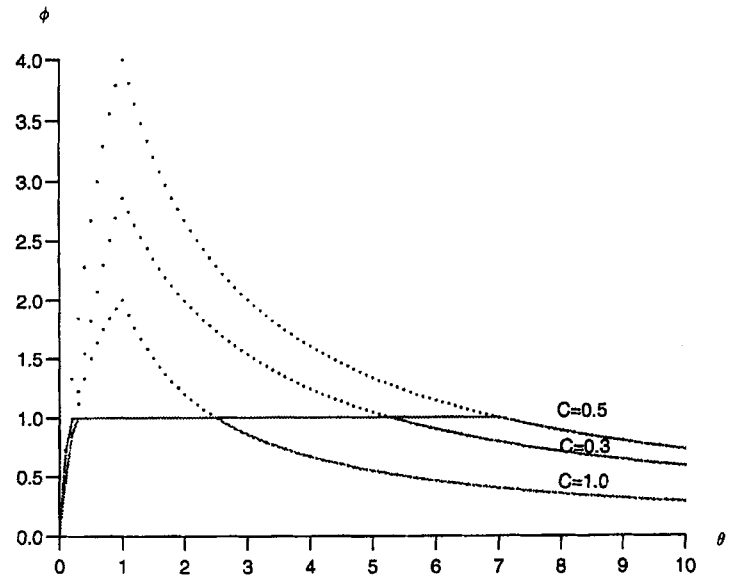

Figure 9. FD3A limiter with Courant numbers 0·1, 0·3 an d0·5 (lines)

Figures 13 and 14 show the comparison of the numerical results of the FD3B limiter function (symbol) and the exact solution (line) after 50 and 1000 time steps respectively with Courant numbers 0·5, 0·7 and 0·9. The numerical results of FD3B are superior to those obtained with FD3A. There is virtually no numerical diffusion, but some tendency to 'square' the smooth parts is observed. For $|c|$ close to $\frac{1}{2}$ the results are very accurate for both the smooth and discontinuous parts of the solution. We can expect that the fully discrete third-order flux limiter scheme (FD3B) will give good performance for most practical flows.

6. FOURTH-ORDER TVD SCHEME

The five-point fourth-order scheme can be written as

$$F_{j+1/2} = \tfrac{1}{2}(F_j^n + F_{j+1}^n) - \frac{|a|}{2}\Delta U_{j+1/2} + (|a|D_0\Delta U_{j+1/2} + |a|D_1\Delta U_{j+L+1/2})\phi_j + |a|D_2\Delta U_{j+M+1/2}\phi_{j+M}, \tag{61}$$

where D_0, D_1, D_2 are determined by (17). The limiter functions are determined by equations (19)–(22).

Figure 15 shows the TVD regions of the scheme for $\theta_j^* = 1$. The figure has similar features to those of the third-order scheme.

Based on the general TVD condition for the fourth-order scheme,

$$\phi_j = \begin{cases} \dfrac{(1-|c|)\theta_j}{\eta(D_1\theta j + D_0 - D_2)} & \text{for } 0 \leqslant \theta_j \leqslant \theta^{\mathrm{L}}, \\ 1 & \text{for } \theta^{\mathrm{L}} \leqslant \theta_j \leqslant \theta^{\mathrm{R}}, \\ \dfrac{1-|c|+\eta D_1\phi_{j+M}/\theta_j^*}{\eta(D_0+D_1\theta_j)} & \text{for } \theta_j > \theta^{\mathrm{R}}, \\ 0 & \text{for } \theta_j < 0, \end{cases} \tag{62}$$

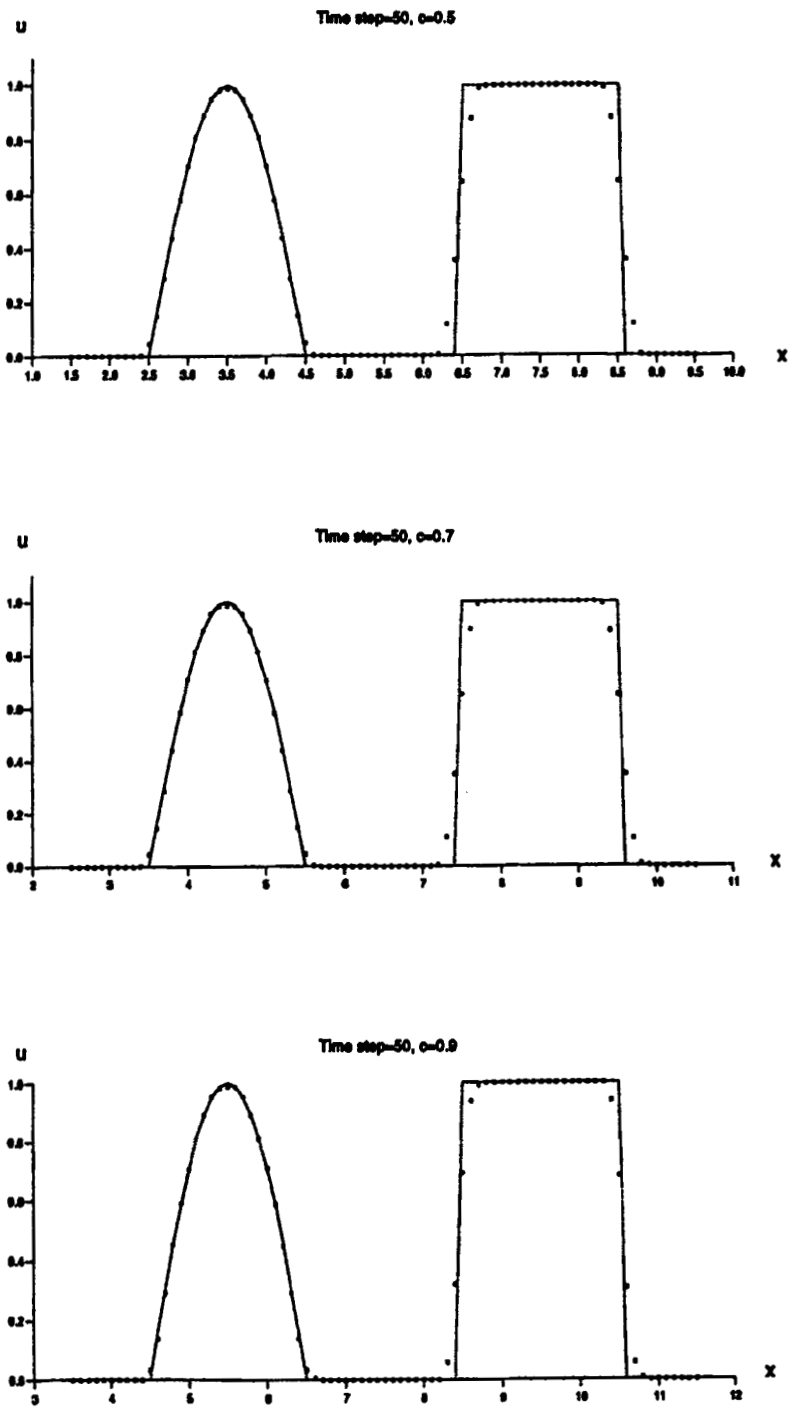

Figure 10. Comparison between exact solution (line) and numerical results of FD3A (symbol) after 50 time steps

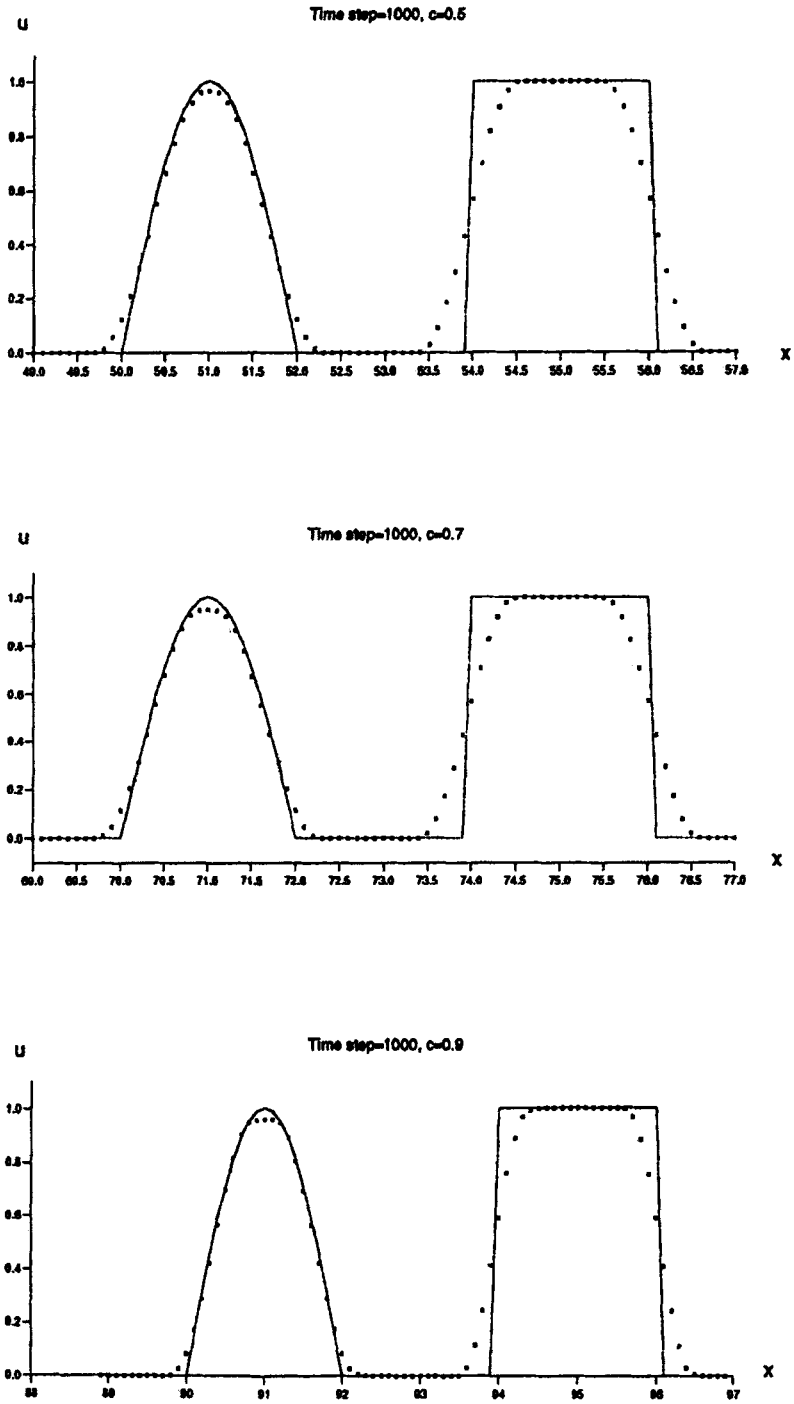

Figure 11. Comparison between exact solution (line) and numerical results of FD3A (symbol) after 1000 time steps

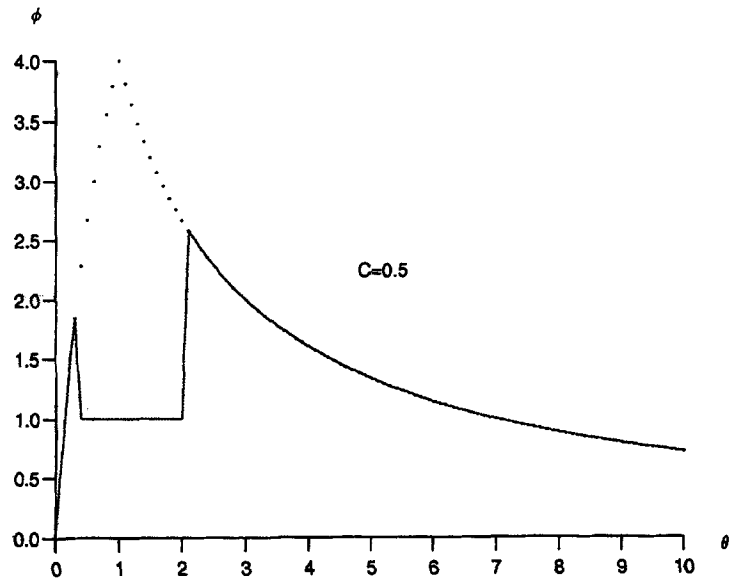

Figure 12. FD3B limiter with Courant number 0·5 (line)

instead of $\phi_{j+M} = 1$ in equation (20) we define

$$\phi_{j+M} = \begin{cases} \eta\theta_{j+M} & \text{for } 0 \leqslant \theta_{j+M} < 0{\cdot}5, \\ 1 & \text{for } \theta_{j+M} > 0{\cdot}5, \\ 0 & \text{for } \phi_j = 0. \end{cases} \tag{63}$$

Our first limiter function called FD4A is obtained by setting

$$\theta^{\mathrm{L}} = \frac{\eta(D_0 - D_2)}{1 - |c| - \eta D_1}, \tag{64}$$

$$\theta^{\mathrm{R}} = \frac{1 - |c| - \eta(D_0 - D_2\phi_{j+M}/\theta_j^*)}{\eta D_1}. \tag{65}$$

Figures 16 and 17 show comparisons between the numerical results (symbol) and the exact solution (line) after 50 and 1000 time steps respectively with Courant numbers 0·5, 0·7 and 0·9. The results indicate that the FD4A limiter is satisfactory for short-time evolution but not for long-time evolution.

Another limiter function called FD4B is obtained by setting θ_j^* and ϕ_{j+M} equal to unity in equation (62) and the choice

$$\theta_{\mathrm{L}} = \eta, \tag{66}$$

$$\theta_{\mathrm{R}} = 3{\cdot}55 - 1{\cdot}5\eta. \tag{67}$$

Figures 18 and 19 show the computed results (symbol) and the exact solution (line). The performance of FD4B is superior to its counterpart FD4A for both short- and long-time evolution, especially for discontinuities. Also, FD4B is simpler than FD4A.

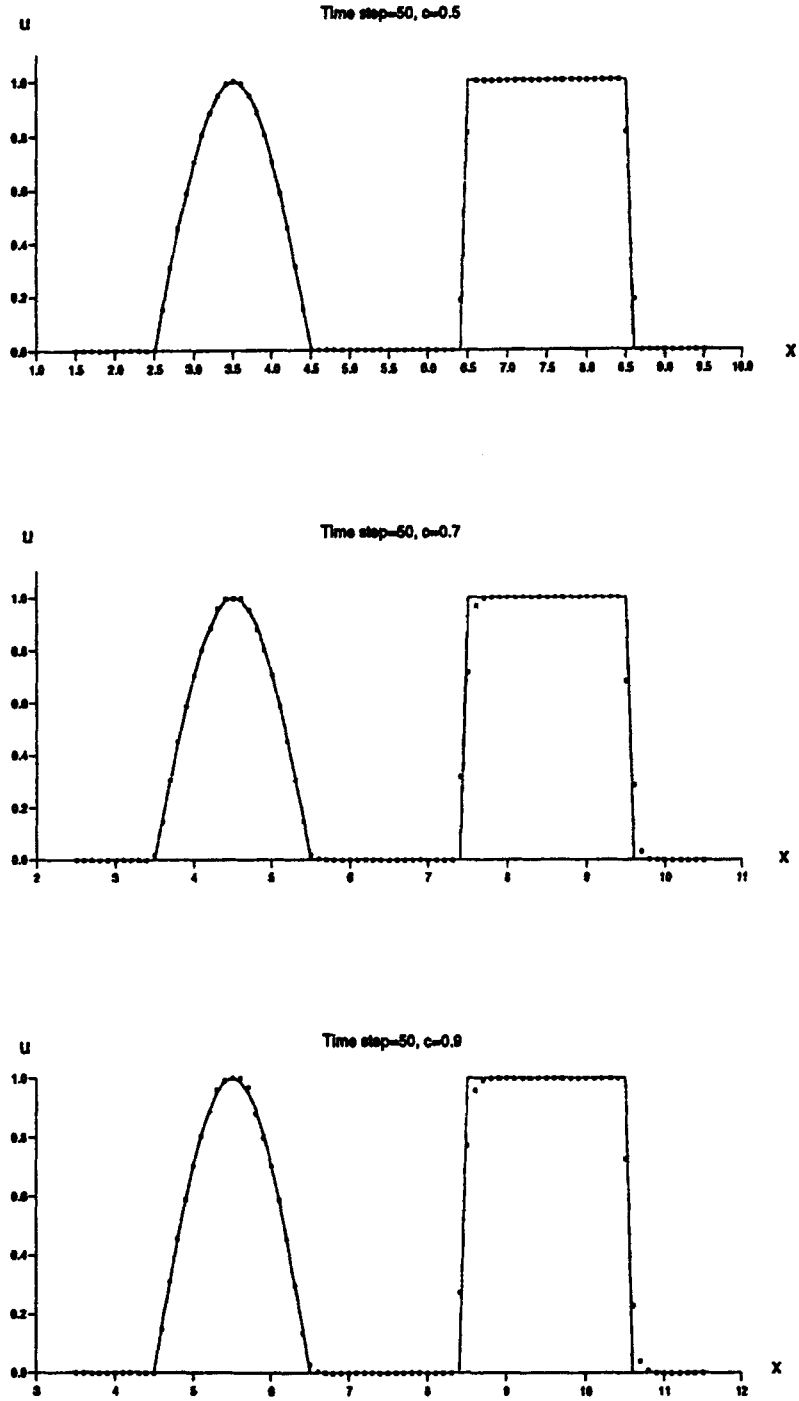

Figure 13. Comparison between exact solution (line) and numerical results of FD3B (symbol) after 50 time steps

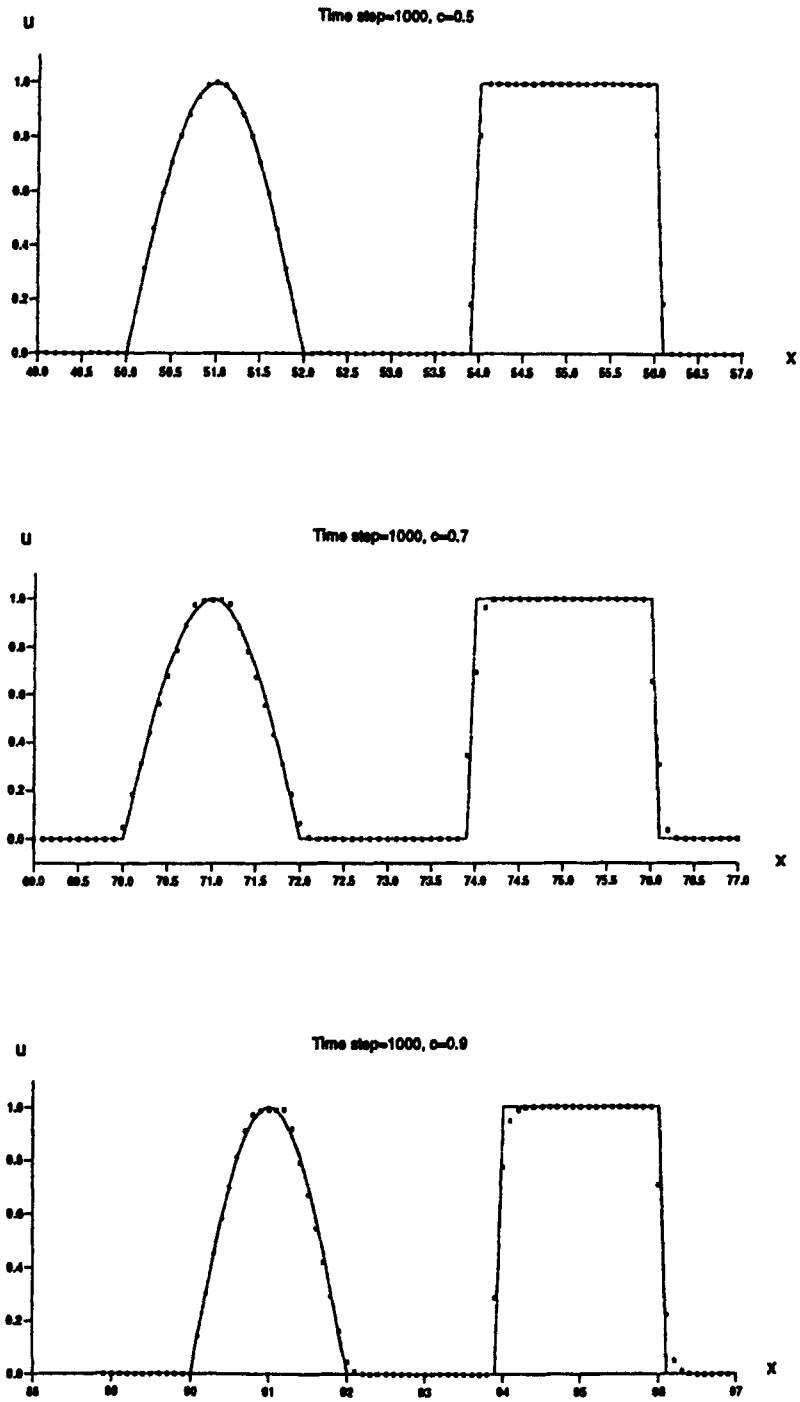

Figure 14. Comparison between exact solution (line) and numerical results of FD3B (symbol) after 1000 time steps

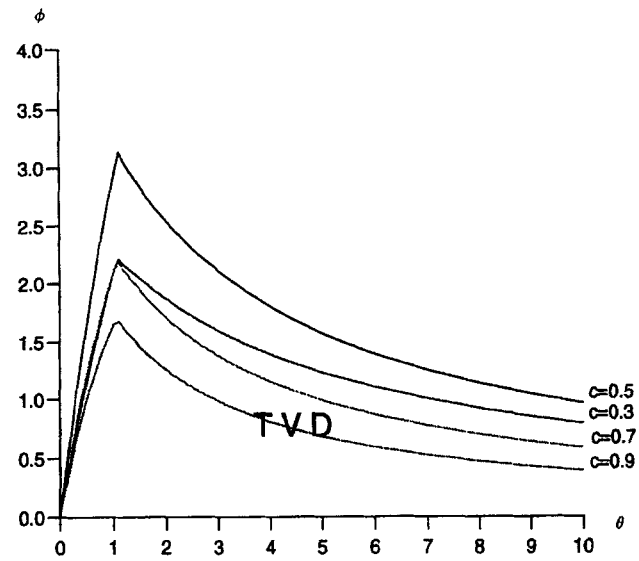

Figure 15. Courant-number-dependent fourth-order TVD region for $\theta_j^* = 1$

7. *H*th-ORDER TVD SCHEMES

In order to obtain *H*th-order TVD schemes, one approach is to use a hybrid flux limiter method following the flux-corrected transport approach[8] whereby the *H*th-order flux can be written as

$$F_{j+1/2} = F_{j+1/2}^{(L)} + \left(F_{j+1/2}^{(H)} - F_{j+1/2}^{(L)}\right)\phi_j^*, \tag{68}$$

where $2 \leqslant L \leqslant 4, H > 4$ and $F_{j+1/2}^{(L)}$ is the *L*th-order flux which includes a rigorously derived limiter ϕ_j. Here ϕ_j^* is an empirical flux limiter which is unity in smooth regions and makes the flux (68) *H*th-order-accurate. In regions of high gradients, ϕ_j^* is zero, which means that the flux (68) reduces to the *L*th-order scheme with an appropriate limiter.

In order to determine ϕ_j^*, we need first to define the locally smooth regions for flux (68). We utilize the information provided by the *L*th-order TVD method. For example, for the third-order method with FD3A limiter (Figure 9) the 'smooth' regions is given by equation (56), i.e.

$$\frac{\eta(2 - |c|)}{6 - \eta(1 + |c|)} \leqslant \theta_j \leqslant \frac{6 - \eta(2 - |c|)}{\eta(1 + |c|)}.$$

To validate the empirical approach of (68) for high-order methods, we consider

$$F_{j+1/2} = F_{j+1/2}^{(3)} + \left(F_{j+1/2}^{(4)} - F_{j+1/2}^{(3)}\right)\phi_j^* \tag{69}$$

($L = 3, H = 4$ in equation (68)). The results of the scheme can be compared directly with those of the fourth-order TVD schemes of the previous section.

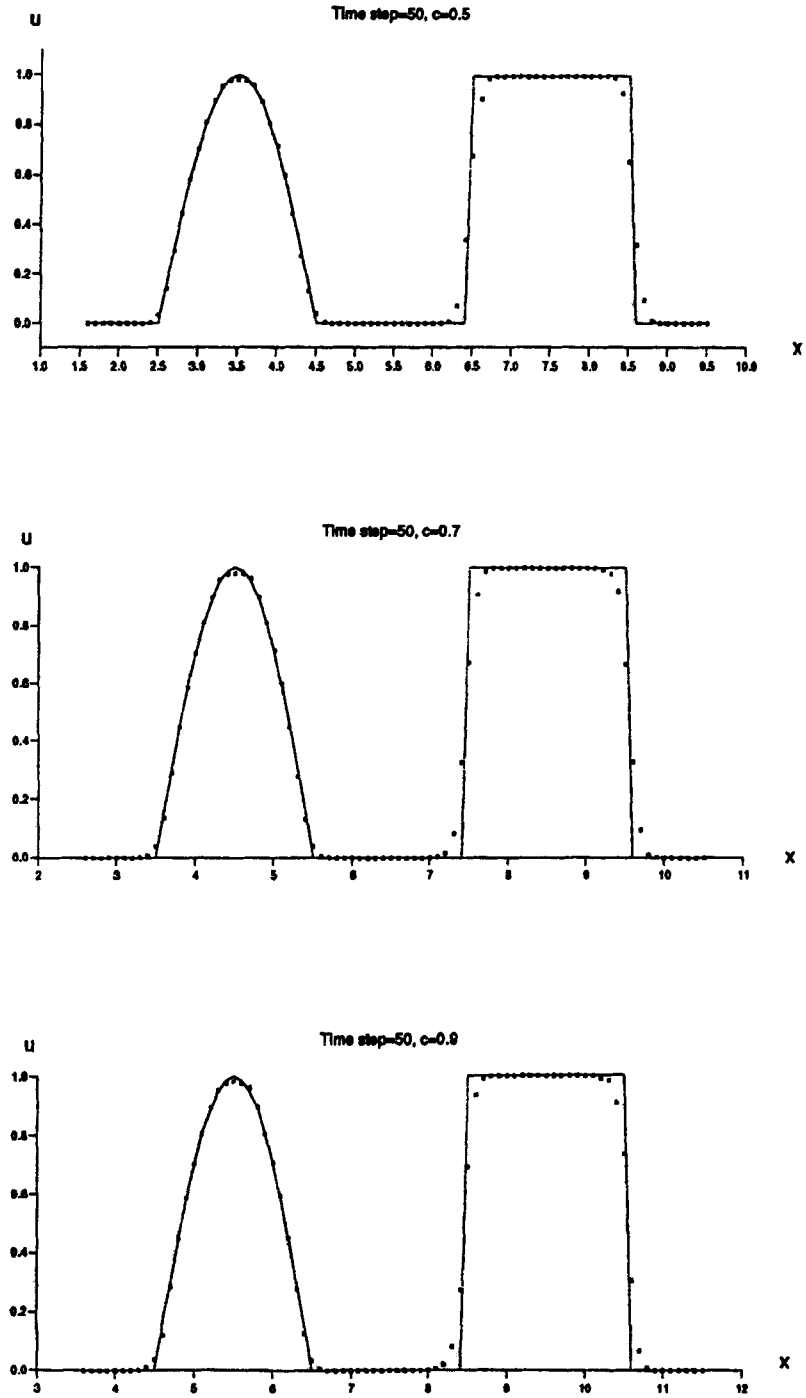

Figure 16. Comparison between exact solution (line) and numerical results of FD4A (symbol) after 50 time steps

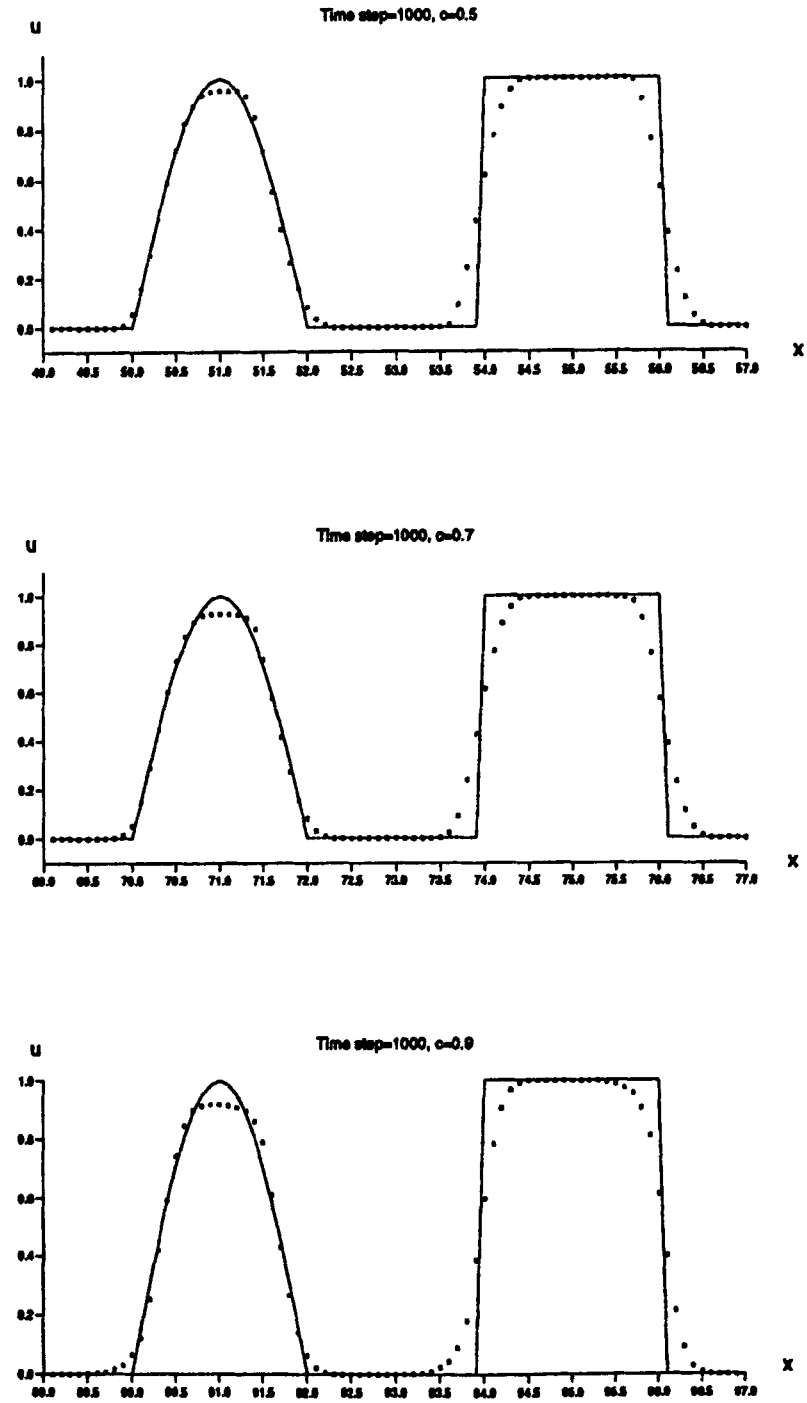

Figure 17. Comparison between exact solution (line) and numerical results of FD4A (symbol) after 1000 time steps

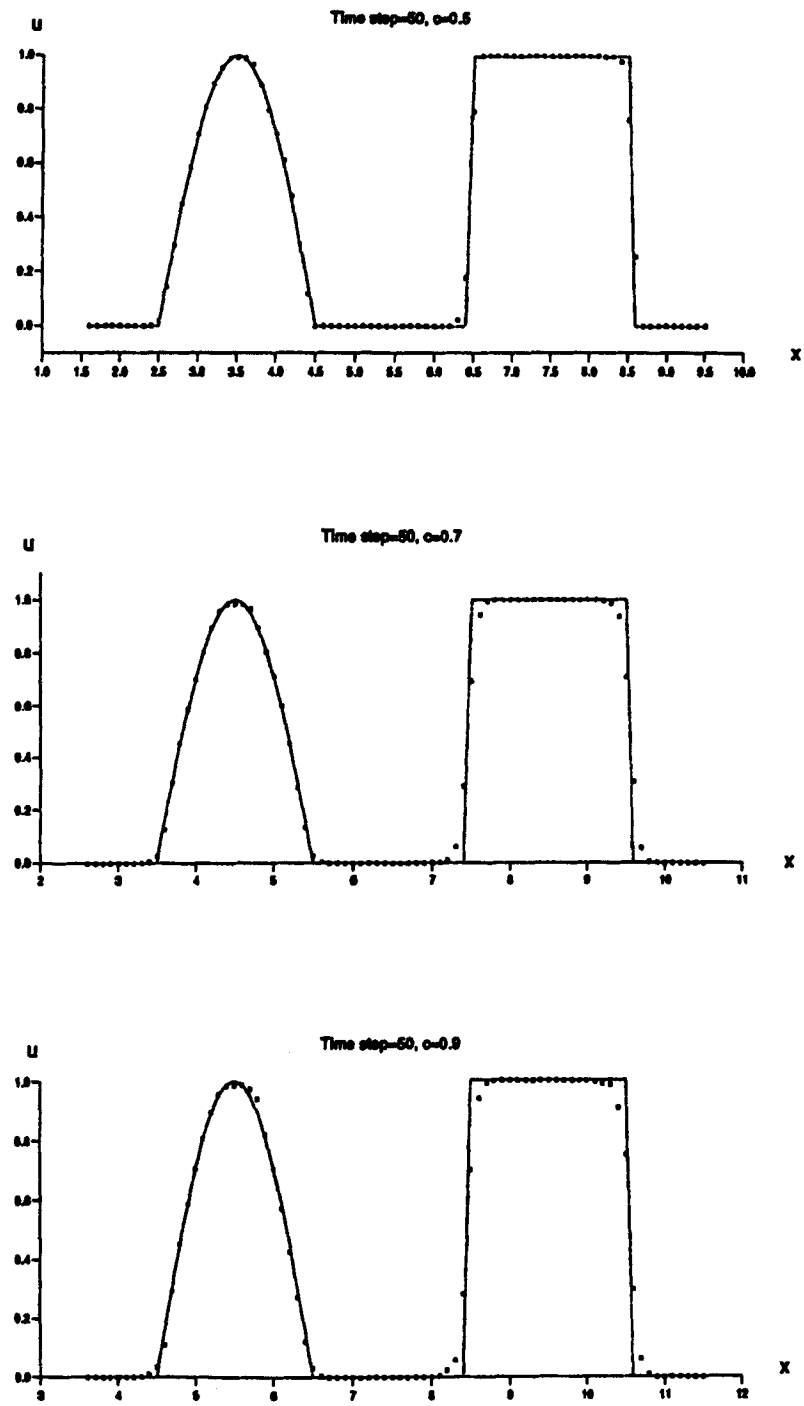

Figure 18. Comparison between exact solution (line) and numerical results of FD4B (symbol) after 50 time steps

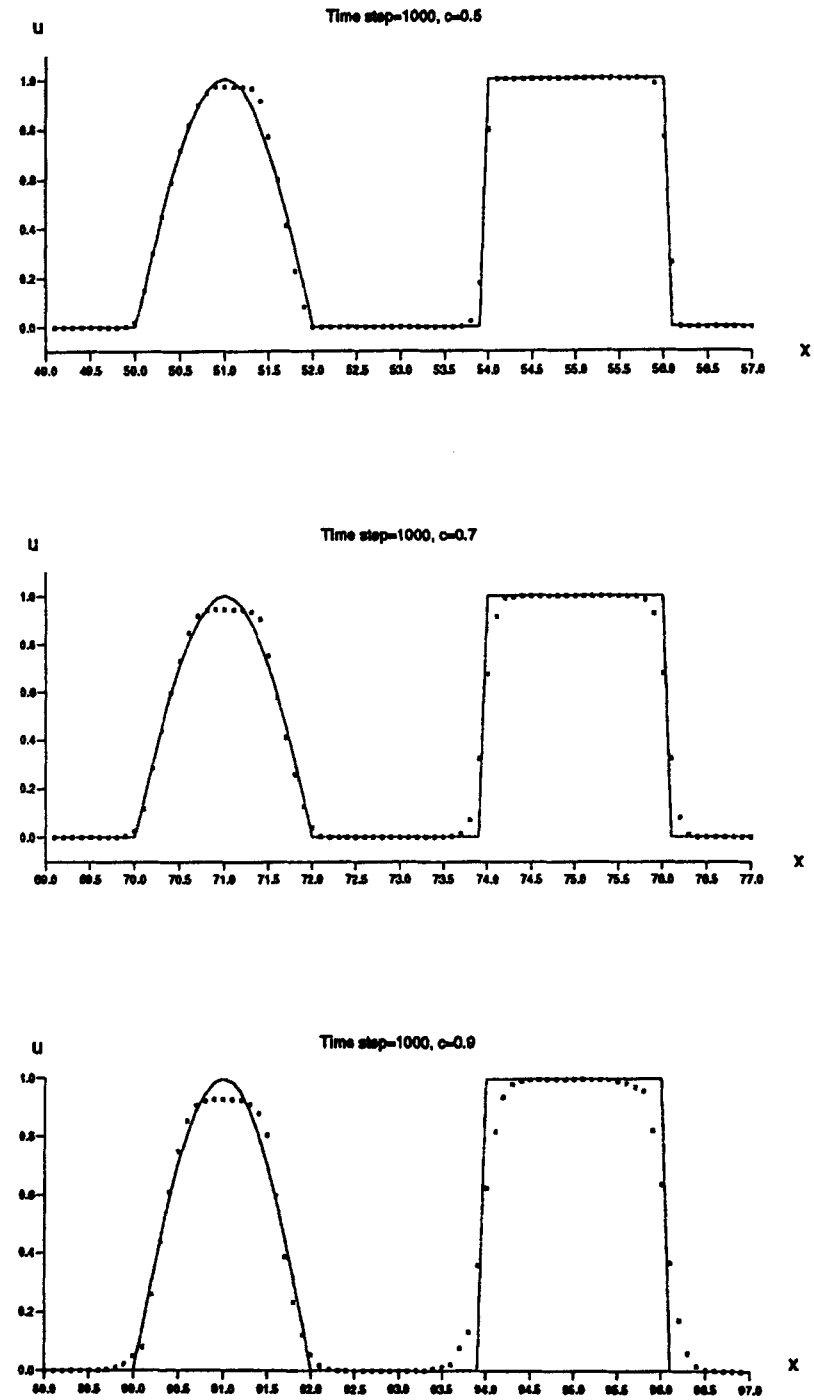

Figure 19. Comparison between exact solution (line) and numerical results of FD4B (symbol) after 1000 time steps

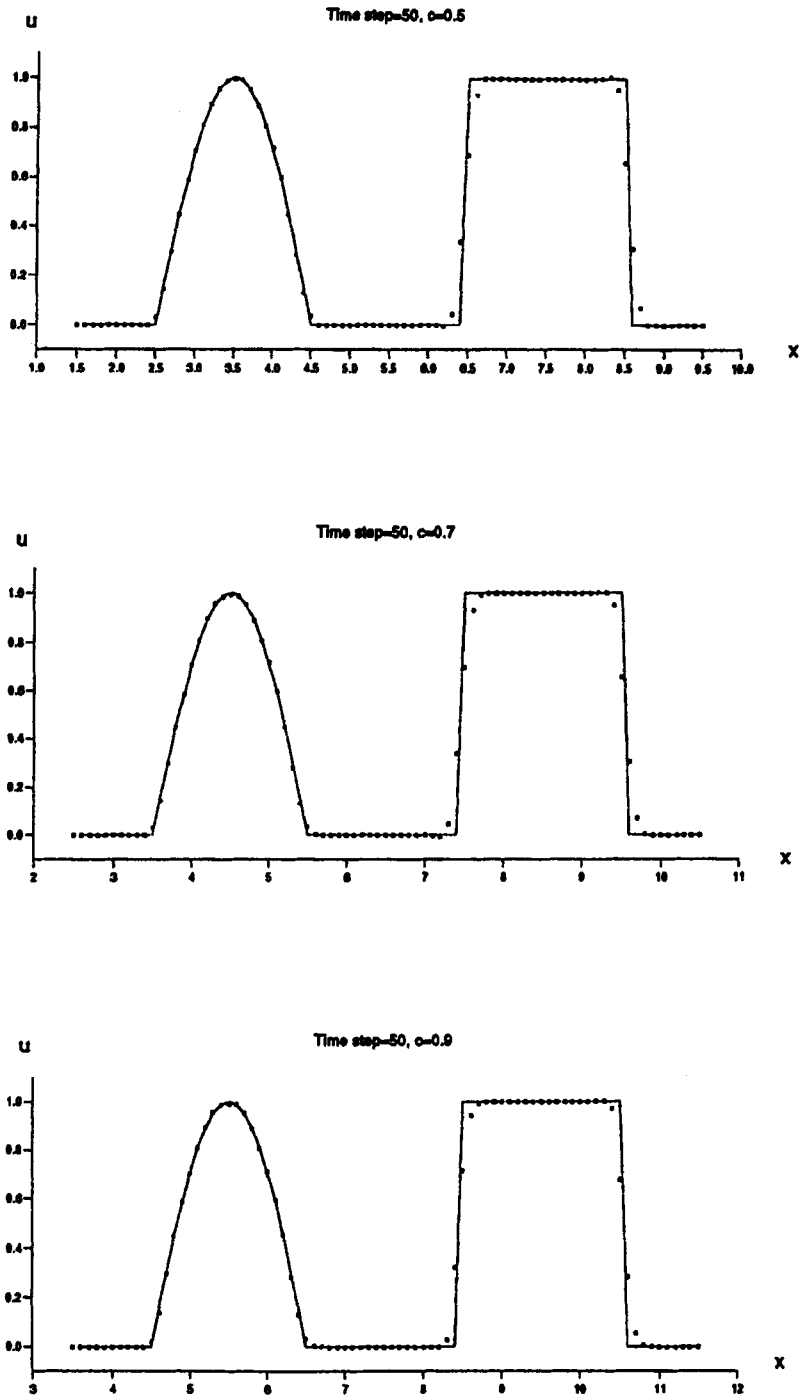

Figure 20. Comparison between exact solution (line) and numerical results of hybrid fourth-order method (symbol) after 50 time steps

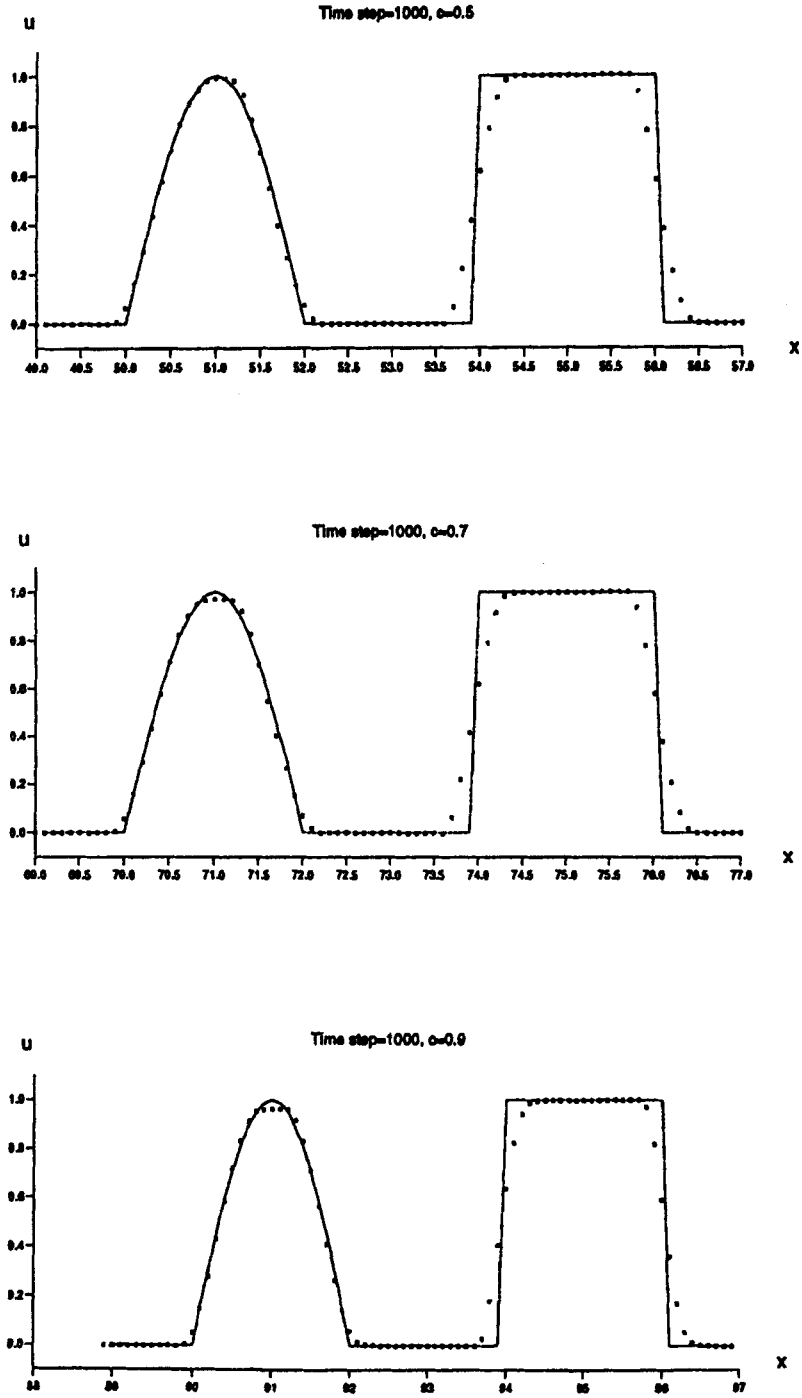

Figure 21. Comparison between exact solution (line) and numerical results of hybrid fourth-order method (symbol) after 1000 time steps

Since the flux (69) involves three intercell boundaries $(j-\frac{1}{2}, j+\frac{1}{2}, j+\frac{3}{2})$, locally smooth regions for flux (69) mean that in all these cells the flow parameters θ_j^s must be indicative of smooth flows. Therefore the empirical flux limiter ϕ_j^* is determined by

$$\phi_j^* = 1 \quad \text{if} \begin{cases} \dfrac{\eta(2-|c|)}{6-\eta(1+|c|)} \leqslant \theta_j^1 \leqslant \dfrac{6-\eta(2-|c|)}{\eta(1+|c|)}, \\ \dfrac{\eta(2-|c|)}{6-\eta(1+|c|)} \leqslant \theta_j^2 \leqslant \dfrac{6-\eta(2-|c|)}{\eta(1+|c|)}, \end{cases} \tag{70}$$

$$\phi_j^* = 0 \quad \text{otherwise}, \tag{71}$$

where

$$\left.\begin{aligned} \theta_j^1 &= \Delta U_{j-1/2}/\Delta U_{j+1/2} \\ \theta_j^2 &= \Delta U_{j+1/2}/\Delta U_{j+3/2} \end{aligned}\right\} \quad \text{for } c > 0, \qquad \left.\begin{aligned} \theta_j^1 &= \Delta U_{j+3/2}/\Delta U_{j+1/2} \\ \theta_j^2 &= \Delta U_{j+1/2}/\Delta U_{j-1/2} \end{aligned}\right\} \quad \text{for } c < 0. \tag{72}$$

Figures 20 and 21 show comparisons between the exact solution (line) and the numerical results (symbol) obtained by the empirical TVD version of the fourth-order scheme with flux (69) after 50 and 1000 time steps respectively. It is instructive to compare these results with those obtained by the rigorous TVD fourth-order schemes of Figures 16 and 17 (obtained with the FD4A limiter) and Figures 18 and 19 (obtained with the FD4B limiter). The TVD condition appears to be more restrictive on the fourth-order scheme than on the third-order scheme. The higher-order method has a wider stencil and thus has the potential for becoming first-order-accurate (locally) more often than the lower-order scheme.

The hybrid limiting approach of equation (68) provides a satisfactory way of dealing with high-order schemes. The basic scheme $F_{j+1/2}^{(L)}$ is Lth-order-accurate in smooth parts and has a limiter which is theoretically sound. The only empirical aspect comes in the choice of ϕ_j^*, but the approach suggested utilizes the throry for the Lth-order scheme to detect smooth regions, in which ϕ_j^* is set to unity, giving in this way the Hth-order scheme.

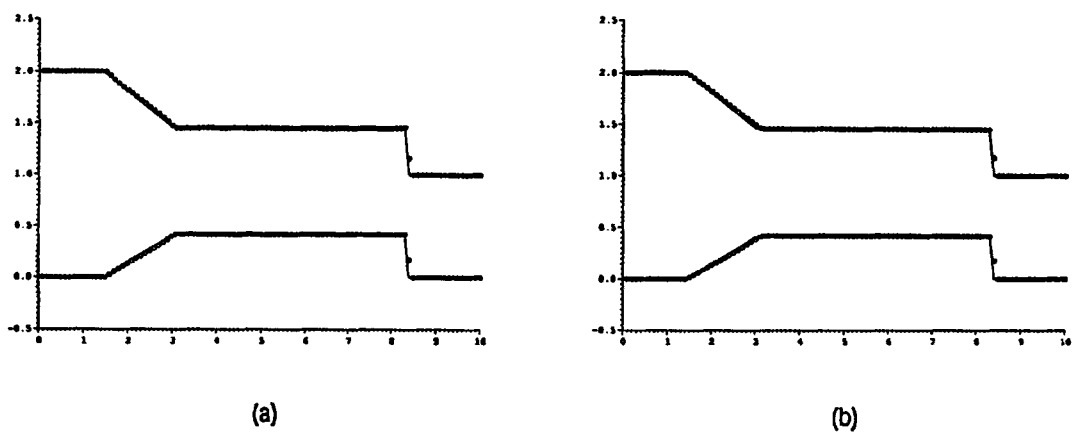

(a) (b)

Figure 22. Dam-break problem by second-order scheme: (a) with FD2A limiter function; (b) with FD2B

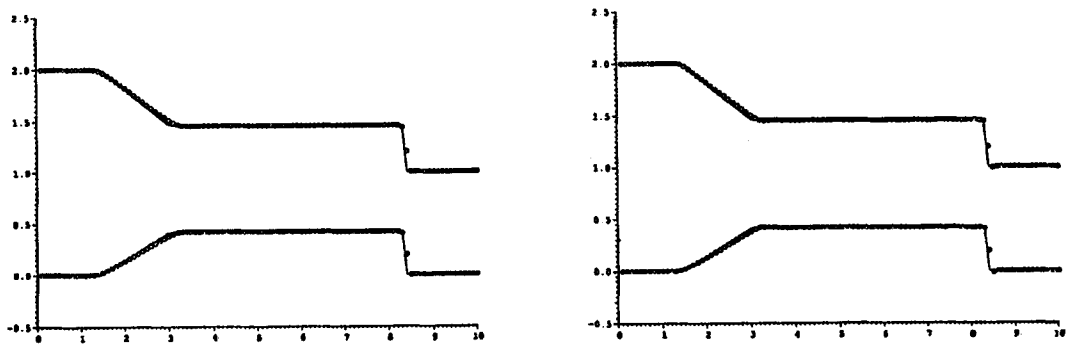

(a) (b)

Figure 23. Dam-break problem by third-order scheme: (a) with FD3A limiter function; (b) with FD3BB

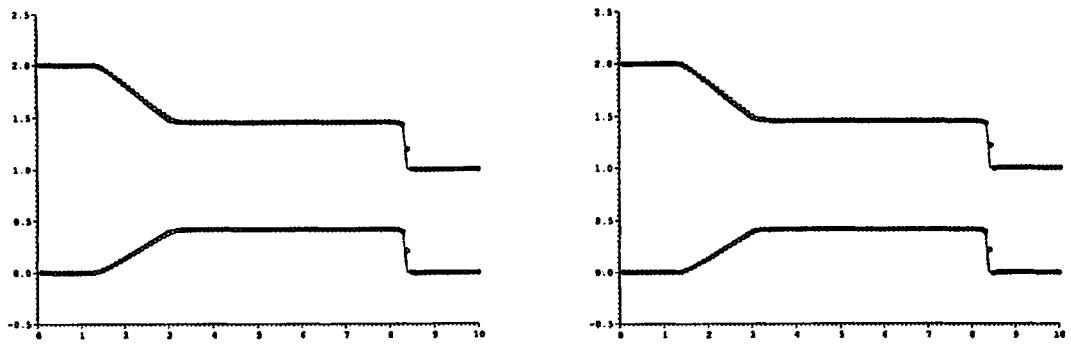

(a) (b)

Figure 24. Dam-break problem by fourth-order scheme: (a) with FD4A function; (b) with FD4B

8. NON-LINEAR HYPERBOLIC SYSTEMS

In this section we discuss the extension of the high-order schemes to non-linear systems of conservation laws. We take the one-dimensional shallow water equations as a typical non-linear system of conservation laws,

$$\begin{bmatrix} \varphi \\ \varphi u \end{bmatrix} + \begin{bmatrix} \varphi u \\ \varphi u^2 + \frac{1}{2}\varphi^2 \end{bmatrix} = \begin{bmatrix} 0 \\ 0 \end{bmatrix}, \tag{73}$$

$$\varphi = gh, \tag{74}$$

where u is the particle velocity, $g = 9{\cdot}8$ m s^{-2} is the gravitational acceleration and h is the depth of the shallow water.

The system of equations (73) is hyperbolic. The eigenvalues of the Jacobian matrix are

$$\lambda^{(1)} = u - a, \qquad \lambda^{(2)} = u + a, \tag{75}$$

where $a = \sqrt{\varphi}$ is the celerity (analogous to the sound speed).

We validate the high-order TVD schemes by solving shallow water equations (73) that simulate a dam-break problem with data

$$(\varphi, u) = \begin{cases} (2, 0), & 0 \leqslant x \leqslant 5, \\ (1, 0), & 5 < x \leqslant 10. \end{cases} \tag{76}$$

Figures 22–24 show the comparison between the exact solution (line) and the computed results (symbols) using the exact Riemann solver at time $t = 2{\cdot}5$ with second-, third- and fourth-order schemes respectively. The computational domain is divided into 100 computational cells. The Courant number used is 0·8. In each figure the top plot shows the free surface profile in terms of the variable φ and the bottom plot shows the particle velocity u-distribution. As can be seen, all schemes can properly capture the features of the flow, i.e. the right-travelling bore and the left depression wave.

9. CONCLUSIONS AND DISCUSSION

Courant-number-dependent TVD regions for second-, third- and fourth-order schemes have been theoretically established. Some simple flux limiter functions have been proposed and tested via numerical experiments. For methods of Hth-order accuracy ($H > 4$) we propose a semiempirical limiting procedure that appears to work well. Tests on the case $H = 4$ give very satisfactory results. The extension of these schemes to systems of non-linear hyperbolic conservation laws has been illustrated by solving the 1D shallow water equations.

Although some simple flux limiter functions have been presented in the paper, we expect better limiters to emerge, such as the van Leer[9,10] and van Albada[11] smooth-type limiters based on the Courant-number-dependent TVD regions. A theory is needed which can rigorously prove that a limiter has a combined property of third- or fourth-order accuracy and monotonicity.

REFERENCES

1. J. Shi and E. F. Toro, 'Fully discrete Arbitrary-order schemes for a model hyperbolic conservation law', College of Aeronautics Report No. 9307, Cranfield University, 1993
2. L. N. Trefethen, 'Group velocity in finite difference schemes', *SIAM Rev.*, **24**, 113–136 (1982).
3. A. Harten, 'High resolution scheme for hyperbolic conservation laws', *J. Comput. Phys.*, **49**, 357–393 (1983).
4. P. K. Sweby, 'High resolution schemes using flux limiters for hyperbolic conservation laws', *SIAM J. Numer. Anal.*, **21**, 995–1011 (1984).
5. P. L. Roe, 'Approximate Riemann solvers, parameters vectors and difference schemes', *J. Comput. Phys.*, **43**, 357–372 (1981).
6. B. P. Leonard, 'Universal limiter for transient interpolation modelling of the advective transport equations: the ULTIMATE conservation difference scheme', *NASA Tech. Memor. 100916*, 1988.
7. P. L. Roe, 'Generalized formulation of TVD Lax–Wendroff schemes', *NASA Contractor Rep. 84–53*, 1984.
8. J. P. Boris and D. L. Book, 'Flux corrected transport I, SHASTA, a fluid transport algorithm that works', *J. Comput. Phys.*, **11**, 38–69 (1973).
9. V. van Leer, 'Towards the ultimate conservative difference scheme 2. Monotonivity and conservation combined in a second-order scheme', *J. Comput. Phys.*, **14**, 361–370 (1974).
10. V. van Leer, 'Towards the ultimate conservative difference scheme 4. A new approach to numerical convection', *J. Comput. Phys.*, **23**, 276–299 (1977).
11. G. D. van Albada, B. van Leer and W. W. Roberts, 'A comparative study of computational methods in cosmic gas dynamics', *Astron. Astrophys.*, **108**, 76–84 (1982).